ACS OMEGA

Open Access

http://pubs.acs.org/journal/acsodf

Article

Polydopamine-Modified Titanium Dioxide Nanotube Arrays Doped with Calcium as a Sustained Drug Delivery System

Lizhong Wu,[§] Xing Wu,[§] Linzhao Wu, Dongdong Chen, Tao Zhang,* Hong Zheng,* and Xiufeng Xiao*

Cite This: *ACS Omega* 2024, 9, 4949−4956

Read Online

ACCESS | Metrics & More | Article Recommendations

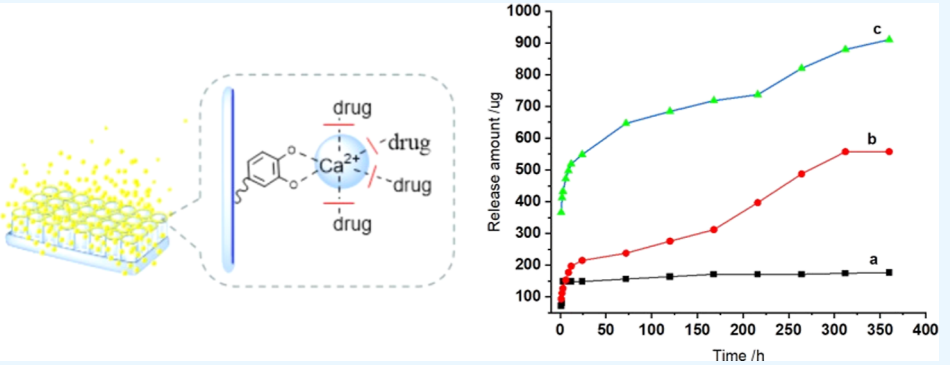

ABSTRACT: Titanium nanotube (TNT) arrays manufactured via electrochemical anodization have been widely used as local drug carriers due to their excellent biocompatibility and customizable nanotubular structures. However, the uncontrollable and abrupt drug release at the early stage decreases the drug release duration, leading to excessive drug concentration at the implantation site. In this study, a continuous drug delivery system based on TNTs was created. Initially, a basic ultrasound-assisted approach was utilized to deposit a polydopamine (PDA) coating onto TNTs to obtain PDA-modified TNTs. Next, TNTs-PDA were submerged in a calcium chloride solution to include Ca^{2+} through Ca^{2+} coordination between the PDA layer's catechol groups. Sodium alendronate (NaAL) was used as a model drug and loaded onto TNTs-PDA-Ca^{2+} by immersing them in an NaAL solution. In the final step, NaAL was covalently attached to TNTs-PDA-Ca^{2+} through coordination bonds with Ca^{2+}. The samples underwent characterization through the use of various techniques, including field emission scanning electron microscopy, Fourier-transform infrared spectroscopy, X-ray diffraction patterning, X-ray photoelectron spectroscopy, and inductively coupled plasma emission spectrometry. The results indicated that the bioactivity of TNTs improved, and there was an enhancement in drug loading capacity and release performance due to modification with PDA and Ca^{2+}. Furthermore, acidic conditions can cause significant drug release due to the cleavage of coordination bonds between the drug and Ca^{2+} ions. Thus, the aforementioned drug delivery system represents a potentially promising approach for achieving sustained and controllable drug release.

1. INTRODUCTION

Dental and orthopedic implants have been clinically treated with titanium and its alloys due to their desirable properties, including excellent corrosion resistance, exceptional biocompatibility, and favorable mechanical properties.[1,2] Nevertheless, Ti-based implants have certain limitations, such as unsatisfactory wear resistance and poor binding to bone tissues, leading to implant loosening and prosthetic joint infections.[1,3,4] Orthopedic implants are still associated with severe complications due to implant-related infections, and long-term drug-eluting medical implants have emerged as a promising solution to tackle this issue. Self-ordered electrochemical anodization of Ti-based implant surfaces has led to the development of titanium nanotube (TNT) arrays that exhibit enhanced bioactivity and bone-binding ability.[5,6] Adjustable nanotubular structures and increased surface area make them an attractive candidate for local drug elution.[7] Drug release behaviors of TNTs conform to the diffusion process and are defined by Fick's laws.[8] Fick's laws state that the diffusion process of drug molecules is influenced by the characteristics of drug molecules such as size, charge, dissolution, and interactions with TNTs.[8−10] Several strategies have been employed to design flexible drug-eluting behaviors suited for different drugs and therapies tailored to their specific requirements. Reportedly,

Received: November 4, 2023
Revised: December 19, 2023
Accepted: January 8, 2024
Published: January 19, 2024

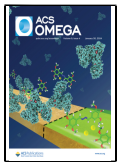

https://doi.org/10.1021/acsomega.3c08772
ACS Omega 2024, 9, 4949−4956

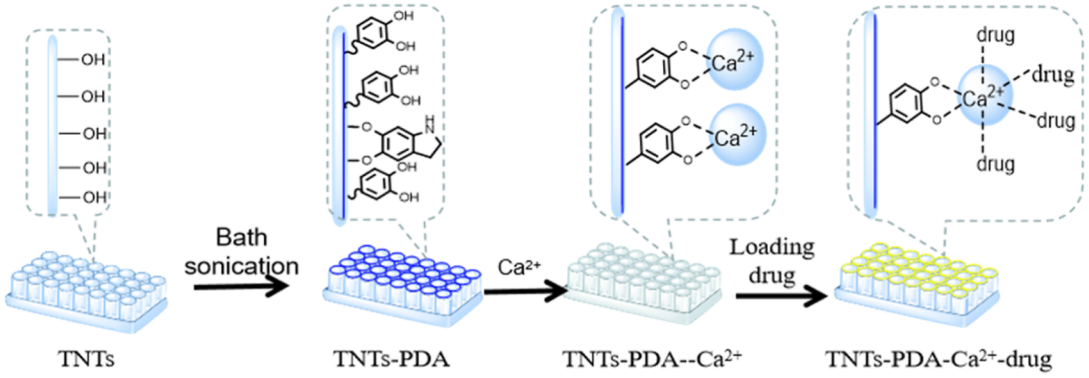

Figure 1. Schematic illustration of the drug delivery system.

strategies for controlling drug release from TNTs include controlling TNT diameters and length, modifying surface chemistry to change hydrophilicity, hydrophobicity, and charge, adjusting TNT openings with coatings, encapsulating drugs with polymeric micelles, or proposing stimulated drug delivery.[8,11−14] Zhao et al. designed a new drug delivery system with an NIR-triggered hydrophobic top layer. The top layer triggers TNT photocatalytic activity and acts as a cap to inhibit drug release. The hydrophilic bottom layer was modified with (3-glycidoxypropyl) trimethoxysilane (GPMS) to introduce amino groups for covalently linking drugs. Reactive oxygen species-induced chain scission under 980 nm laser irradiation could trigger drug release.[15] Long-term drug-eluting medical implants require sustained and controlled drug delivery, which are crucial characteristics.

Polydopamine (PDA) is a new material that can be firmly bonded to various substrates through oxidative self-polymerization of dopamine.[16−18] The materials modified with PDA exhibit a superior ability to attach various functional molecules by utilizing the abundant amino and hydroxyl functional groups present in PDA.[19] Hence, TNTs modified using PDA demonstrate an improved capacity for loading drugs and releasing them.[16,20] Yang and colleagues deposited multiple layers of PDA onto TNTs. As a result, the PDA-modified TNTs demonstrated a higher drug loading capacity and an extended period for elution. Furthermore, the release behavior of the drug can be further regulated by controlling the thickness of the PDA layer.[16]

Based on the above research, a sustained drug delivery system was generated by modifying TNTs using PDA, with the help of the abundant functional groups of PDA and the coordination of metal calcium ions, and sodium alendronate (NaAL) was loaded by coordination with calcium ions as a bridge. NaAL [(4-amino-1-hydroxybutylidene)diphosphonic acid monosodium salt trihydrate] is one of the widely used bisphosphonates for suppressing bone resorption and promoting bone formation.[25] In brief, the inner wall of TNTs was coated with PDA, followed by immersion in a calcium chloride solution to incorporate Ca^{2+} (Figure 1). Calcium ions are crucial for the process of biomineralization, an important process for bone regeneration.[21−23] PDA can form through dopamine self-polymerization, which introduces active sites on the surface, where different functional molecules can be grafted. Calcium ions can be firmly immobilized into TNTs through Ca^{2+} coordination between the catechol groups of the PDA layer.[24] NaAL can be firmly attached to TNTs-PDA-Ca^{2+} through a Ca^{2+} coordination bond.[26] Therefore, the as-prepared TNTs-PDA-Ca^{2+} exhibit enhanced drug loading capacity, sustained-release properties, and improved bioactivity.

2. EXPERIMENTAL SECTION

2.1. Preparation of TNTs. TiO_2 nanotube arrays were produced by simple electrochemical anodization on pure Ti foils. The Ti foils, measuring 10 × 20 × 0.6 mm, were briefly polished and sonicated in acetone for 15 min. Subsequently, the Ti foils were etched with a 5 M nitric acid solution (containing 4 wt % HF) for 10 s and then sonicated in deionized water for 15 min. After drying, a cleaned Ti foil and a Pt foil were placed at the anode and the cathode. After that, the samples underwent anodization for 24 h in an electrolyte (glycerol as the main solvent, containing 0.50 wt % NH_4F and 10 vol % deionized water) under a constant voltage of 60 V. Finally, the TiO_2 nanotube arrays were annealed at 450 °C for 2 h and labeled as TNTs.

2.2. Surface Modification of PDA. TNTs underwent treatment in a 0.5 M NaOH solution at 50 °C for 30 min, followed by cleaning in deionized water and air drying. The treated samples were immersed in a Tris-based buffer solution containing dopamine hydrochloride (0.5 mg/mL) at pH 8.5 and a concentration of 1.2 mg/mL and then subjected to sonication for 12 h.[16] The samples were subsequently labeled as TNTs-PDA after being rinsed with distilled water.

2.3. Calcium Ion Loading and Release. The as-prepared TNTs-PDA were immersed in 0.1 0.5, and 1.0 mol/L calcium chloride solutions at 37 °C for 6 h. Afterward, the samples were gently rinsed in distilled water and dried in the air. TNTs-PDA modified with Ca^{2+} were designated as TNTs-PDA-Ca^{2+}.

2.4. Drug Loading and Release. The various samples were immersed in 30 mg/mL NaAL solution with pH 3.0 for 6 h to load NaAL. Then, they were cleaned gently with distilled water and labeled as TNTs-NaAL, TNTs-PDA-NaAL, and TNTs-PDA-Ca^{2+}-NaAL. The NaAL-loaded samples were incubated in phosphate-buffered saline (PBS) solution with varying pH values of 4.6, 7.4, and 11.0. They were then shaken at a temperature of 37 °C for 15 days. At each predetermined time, a specific volume of the solution was collected and replaced with an equal volume of fresh PBS. The collected solutions were mixed with an equal volume of 1 M $HClO_4$ solution containing 5 mM $FeCl_3$. The concentrations of NaAL were measured using a UV−vis spectrophotometer at a wavelength of 290 nm. The release rate of NaAL for each time interval was calculated, and the corresponding release curve was plotted.

https://doi.org/10.1021/acsomega.3c08772
ACS Omega 2024, 9, 4949−4956

2.5. In Vitro Mineralization Study. The samples were submerged in a 1.5-fold simulated body fluid (1.5 SBF) at 37 °C for 5 days. At specific time intervals, the SBF was entirely replaced with a fresh solution.

2.6. Cell Culture and the Cell Counting Kit-8 Assay. Mouse MC3T3-E1 cells were cultured in MEM Alpha Modification, supplemented with 10% fetal bovine serum and 1% penicillin/streptomycin, at 37 °C in a CO_2 incubator for 24 h. Subsequently, the cells were seeded on the samples and cultured for 1 and 5 days in a 24-well plate at 37 °C. Cell Counting Kit-8 (CCK-8) was added to the culture medium and incubated for 2 h at 37 °C. The cell concentration was subsequently determined by a spectrophotometric microplate reader at a wavelength of 450 nm. Pure unanodized Ti foils were used as a control group.

2.7. Characterization. The surface morphology of the samples was observed by using a field emission scanning electron microscope (JEOL-7500F). The surface chemical composition and chemical states of elements were determined via X-ray photoelectron spectroscopy (XPS, ESCALAB 250). Fourier-transform infrared (FTIR) spectroscopy (Nicolet Avatar 360) was performed to assess the chemical composition of the samples. The amount of calcium ions loaded and released from TNTs-PDA-Ca^{2+}-NaAL was assessed using an inductively coupled plasma emission spectrometer (OPTIMA 8000). The crystal phase composition of the samples was analyzed by X-ray diffraction (XRD, Philips X'Pert MPD).

3. RESULTS AND DISCUSSION

3.1. Characterization of Samples. The morphology of TNTs-PDA-Ca^{2+} and TNTs-PDA-Ca^{2+}-NaAL is presented in Figure 2. TNTs-PDA-Ca^{2+}-NaAL showed a smaller inner diameter of nanotubes (147 ± 10 nm) than TNTs-PDA-Ca^{2+} (inner diameter: 172 ± 10 nm) when observed from the top views as shown in Figure 2a,c. The cross-sectional views of TNTs-PDA-Ca^{2+}-NaAL (Figure 2b) and TNTs-PDA-Ca^{2+} (Figure 2d) show an increase in the thickness and roughness of nanotube walls upon loading with NaAL, whereby it was hypothesized that NaAL had been loaded onto the nanotubes, which was further confirmed by the following methods.

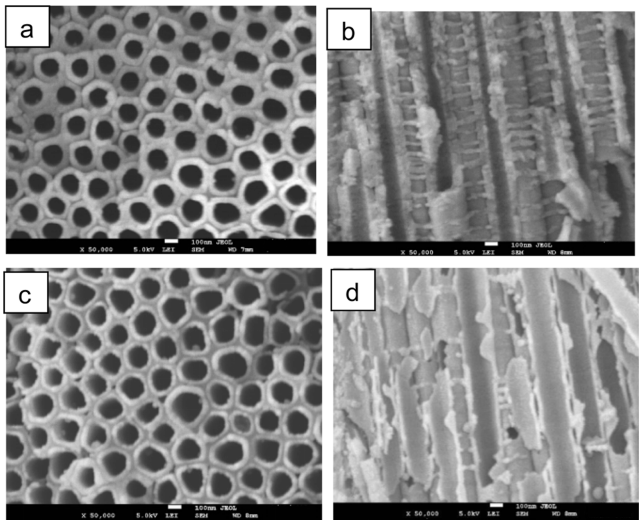

Figure 2. SEM images of (a,b) TNTs-PDA-Ca^{2+}-NaAL (a: top view; b: cross-sectional view) and (c,d) TNTs-PDA-Ca^{2+} (c: top view; d: cross-sectional view).

Figure 3A shows the FTIR spectra of various samples. FTIR spectra of TNTs-PDA-Ca^{2+} showed two peaks at 2919 and 2852 cm^{-1}. These peaks were attributed to the C−H asymmetrical stretching and C−H bending vibrations of PDA, respectively. In addition, two absorption peaks at 1634 and 1498 cm^{-1} were assigned to the C═O and C═N or/and C═C vibrational modes in PDA, as shown in the close-up posting in Figure 3A. These modes are in agreement with previous data for PDA observed by Luo et al.[27] These results indicated the successful deposition of PDA on the surfaces of TNTs. FTIR spectra of TNTs-PDA-Ca^{2+}-NaAL displayed a noticeable absorption peak at 3391 cm^{-1}, which was attributed to the O−H stretching vibration and N−H stretching vibration in amine groups. In addition, the sharp peaks at 1640 cm^{-1} are attributed to the C═O bonds. The absorption peaks at 1128 cm^{-1} are attributed to the characteristic absorption bands of P═O in NaAL.[28,29] Furthermore, P−O bending vibrations were identified at 469 cm^{-1}.[30] These findings suggest a successful loading of NaAL. Additionally, the crystal phase composition of the samples was analyzed by using XRD (Figure 3B). The XRD pattern of TNTs showed diffraction peaks of anatase TiO_2 and Ti metal, and no new diffraction peaks appeared after treatment with PDA and Ca^{2+}. After immersion loading of NaAL, the diffraction peaks of NaAL

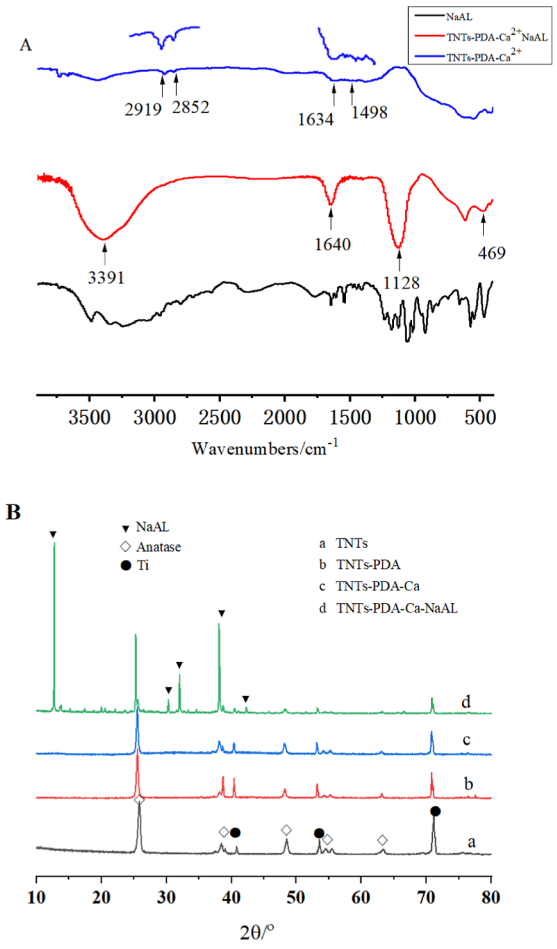

Figure 3. (A) FTIR spectra and (B) XRD patterns of TNTs-PDA-Ca^{2+}, TNTs-PDA-Ca^{2+}-NaAL, and NaAL.

https://doi.org/10.1021/acsomega.3c08772
ACS Omega 2024, 9, 4949−4956

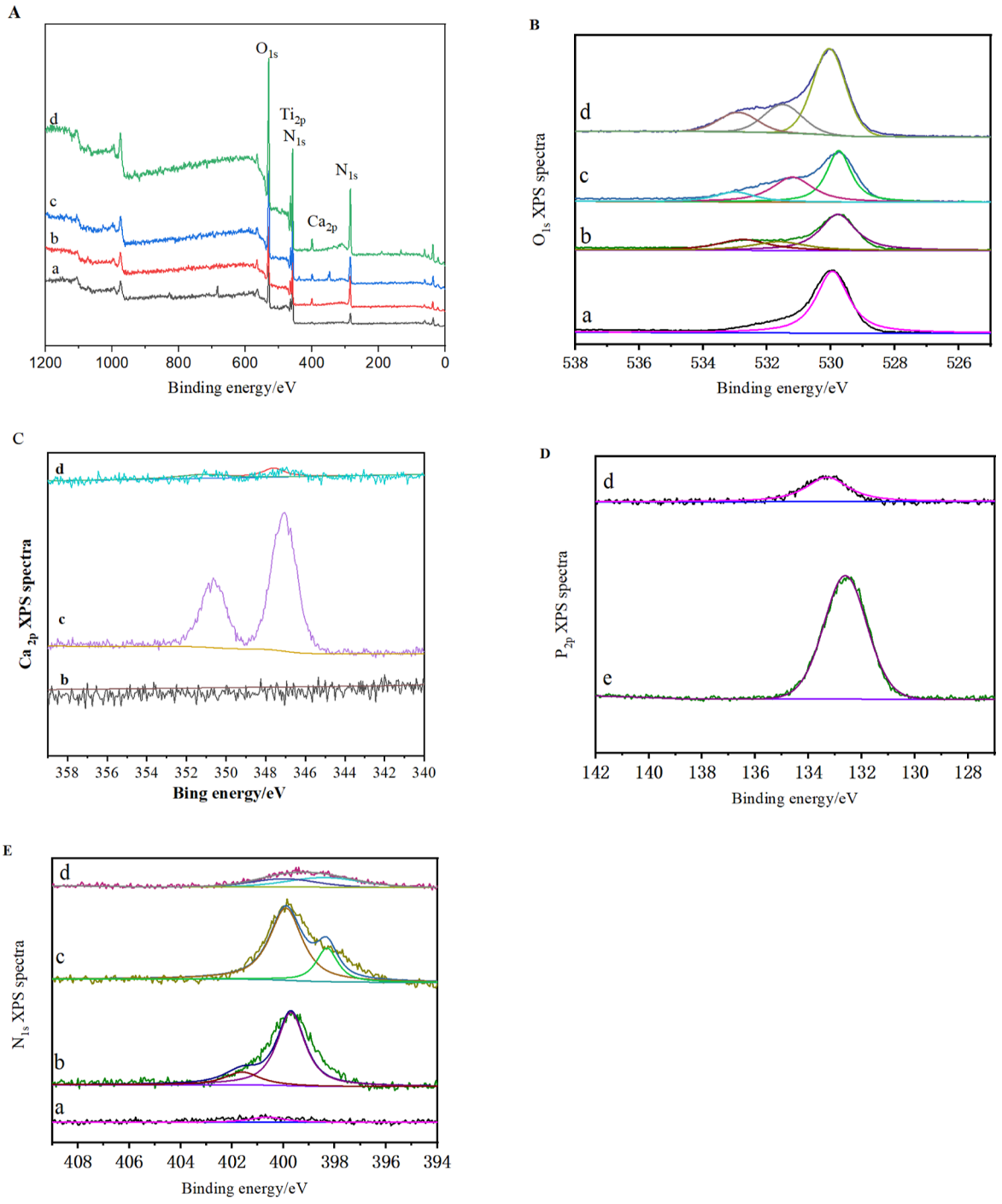

Figure 4. Full XPS spectra (A) and high-resolution XPS spectra of different samples (B) O_{1s}, (C) Ca_{2p}, (D) P_{2p}, and (E) N_{1s} TNTs; (b) TNTs-PDA; (c) TNTs-PDA-Ca^{2+}; (d) TNTs-PDA-Ca^{2+}-NaAL; (e) NaAL.

appeared at 2θ = 12.7, 13.7, 30.3, 31.9, 38.1, and 42.3°, which indicated that the TNTs had been successfully loaded with NaAL.

Additionally, XPS analysis was conducted to further determine the surface chemical composition of the samples. Figure 4A shows the full spectra of different samples, and Figure 4B–E shows the high-resolution spectra of O_{1s}, Ca_{2p}, P_{2p}, and N_{1s}, respectively. The b,c,d spectra of Figure 4A all showed N peaks, indicating that PDA has been modified to the surface of TNTs. Figure 4B is a high-resolution plot of O 1s, and the oxygen-bound state of TNTs [Figure 4B(a)] is mainly a Ti–O bond (529.95 eV, 72.0%), but new peaks appeared after PDA modification of the nanotubes [Figure 4B(b)], which are phenol hydroxyl-C–OH (532.75 eV, 23.9%) and quinone group-C═O (531.6 eV. 20.2%); these results further indicate that PDA has been modified onto the nanotubes. The –C–OH peak area after immersion of calcium ions [Figure 4B(c)] decreased to 15.2%, while the corresponding quinone-based-C═O peak area increased to 37.9%, indicating that PDA chelated calcium ions by conversion from a phenolic hydroxyl group to a quinone group. The line shapes and peak components of the O 1s spectra of the samples [Figure 4B(d)] did not change significantly after loading NaAL.

https://doi.org/10.1021/acsomega.3c08772
ACS Omega 2024, 9, 4949–4956

In the Ca_{2p} high-resolution map, two peaks appeared in sample TNTs-PDA-Ca^{2+} [Figure 4C(c)] relative to sample TNTs-PDA [Figure 4C(b)], 351.0 eV for $Ca_{2p1/2}$ and 347.5 eV for $Ca_{2p3/2}$, which indicated that calcium ions had successfully modified the modified nanotubes and that the PDA chelating of Ca^{2+} did not affect the Ca^{2+} chemical valence state. The sample TNTs-PDA-Ca^{2+}-NaAL [Figure 4C(d)] showed the same presence of $Ca_{2p1/2}$ and $Ca_{2p3/2}$ peaks, whereas the decrease in peak intensity and peak area as well as the displacement of peak position speculated that the sample TNTs-PDA-Ca^{2+} were chemically bonded to the drug NaAL.

In the high-resolution plot of P_{2p}, the electron binding energy of P_{2p} in pure NaAL [Figure 4D(e)] was 132.61 eV, compared to the electron binding energy of P_{2p} in sample TNTs-PDA-Ca^{2+}-NaAL which was 133.37 eV, and the peak position was shifted further speculating that the sample TNTs-PDA-Ca^{2+} interacted with the phosphate in the drug NaAL.

In the high-resolution plot of N_{1s}, N_{1s} of sample TNTs-PDA appeared at 399.7 and 401.6 eV (Figure 4b). It is shown that the N on the surface of the sample exists in two forms, one part in the form of $-NH_2$ and the other part in the form of NH_3^+. All of these results indicate that PDA has been successfully modified onto TiO_2 nanotubes. N_{1s} of sample TNTs-PDA-Ca^{2+} [Figure 4E(c)] appeared at 398.3 and 399.6 eV where the peaks were located, further indicating that the dopamine had been successfully modified onto the nanotubes. While the N_{1s} of sample TNTs-PDA-Ca^{2+}-NaAL [Figure 4E(d)] had the same characteristic peaks at 398.4 and 400.3 eV, N_{1s} peaks were shifted, which was mainly due to the presence of metal ions, which decreased the electron cloud density of N, increased the positive electronegativity of the nucleus, and elevated the binding energy, thus, indicating the successful loading of Ca^{2+} onto nanotubes with drugs through ligand bond interactions.

In order to study the loading of the samples, the samples were subjected to thermogravimetric tests. Figure 5a shows

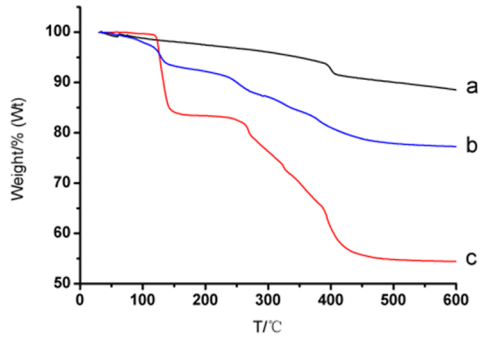

Figure 5. TG curve of the samples: (a) TNTs-PDA; (b) TNTs-PDA-Ca^{2+}-NaAL; (c) NaAL.

that for PDA-modified nanotubes, the weight loss of the sample increases with increasing temperature, which mainly originates from the weight loss of water on the surface of the sample, and the PDA starts to decompose when the temperature reaches 400 °C. Figure 5c shows that for pure NaAL, which loses its water of crystallization between the temperatures of 105 and 145 °C, the decomposition of NaAL starts when the temperature rises to 245 °C, and the temperature lasts until about 455 °C, the sample then reaches almost constant weight. While Figure 5b shows the Ca^{2+}-modified nanotubes loaded with NaAL, the sample loses a large amount of weight between 115 and 155 °C, which is mainly caused by the combined effect of the water of crystallization of NaAL and the adsorbed water on the surface of the sample. There is a significant weight loss at 250−460 °C, which is caused by the decomposition of NaAL and follows the same thermogravimetric trend as curve c for pure NaAL, with a weight loss of 11.87% in this temperature range.

3.2. Drug Release Performance and Drug Release Kinetics Analysis. In order to study the ability of Ca^{2+}-modified nanotubes to slow drug release, the samples were loaded with the same concentration of NaAL and placed in 10 mL of PBS buffer solution with pH = 7.4 for 15 days, and the drug release curves are shown in Figure 6. The drug release process was divided into two phases: rapid release in the early stage and sustained release in the late stage. TNT samples [Figure 6A(a)] released the drug to completion in the rapid release stage in the early stage, indicating that there was only a weak physical adsorption between the drug and the TNTs, and the drug was rapidly released by diffusive dissolution. The release of TNTs-PDA [Figure 6A(b)] and TNTs-PDA-Ca^{2+} [Figure 6A(c)] was both significantly higher than TNTs, and the latter was higher than the former, and the late slow release curves of both were close to a straight line, suggesting that both PDA and Ca^{2+} have chemisorption and electrostatic interactions with the drug to enhance drug loading, as shown by the XPS spectra.

The mechanism of release of NaAL from TNTs-PDA-Ca^{2+}-NaAL was also analyzed. The drug release kinetics from TNTs were studied using three kinetic models: zero-order release equation, first-order release equation, and Higuchi release equation. The equations are displayed in eqs 1, 2, and 3, respectively.[31−33]

$$\text{Zero-order release equation: } \frac{M_t}{M_\infty} = a + kt \tag{1}$$

$$\text{First-order release equation: } \ln 1 - \frac{M_t}{M_\infty} = -kt \tag{2}$$

$$\text{Higuchi release equation: } \frac{M_t}{M_\infty} = kt^{1/2} \tag{3}$$

where M_t represents the cumulative amount of drug release at time t, M_∞ is the total amount of drug release during the whole release process, and a is the initial amount of drug in solution (it is usually zero). $\frac{M_t}{M_\infty}$ represents the fraction of drug released at each time point, and k is the release rate constant.

Figure 6B presents the fitting curve of TNTs-PDA-Ca^{2+}-NaAL at the sustained release stage. The fitted equation is shown in eq 4

$$\frac{M_t}{M_\infty} = 0.39179 + 0.00165t \tag{4}$$

Equation 4 indicates a correlation coefficient (R^2) value of 0.995. Figure 6B displays that the release kinetics during the sustained release stage adheres to the zero-order release profile. The coordinate covalent bonds between NaAL and Ca^{2+} primarily cause a stable release rate.

To investigate the release behaviors of TNTs-PDA-Ca^{2+}-NaAL under different pH conditions, the samples were immersed in PBS solutions with varying pH levels (4.6, 7.4, and 11.0). Figure 6C illustrates the drug release profiles. As can

https://doi.org/10.1021/acsomega.3c08772
ACS Omega 2024, 9, 4949−4956

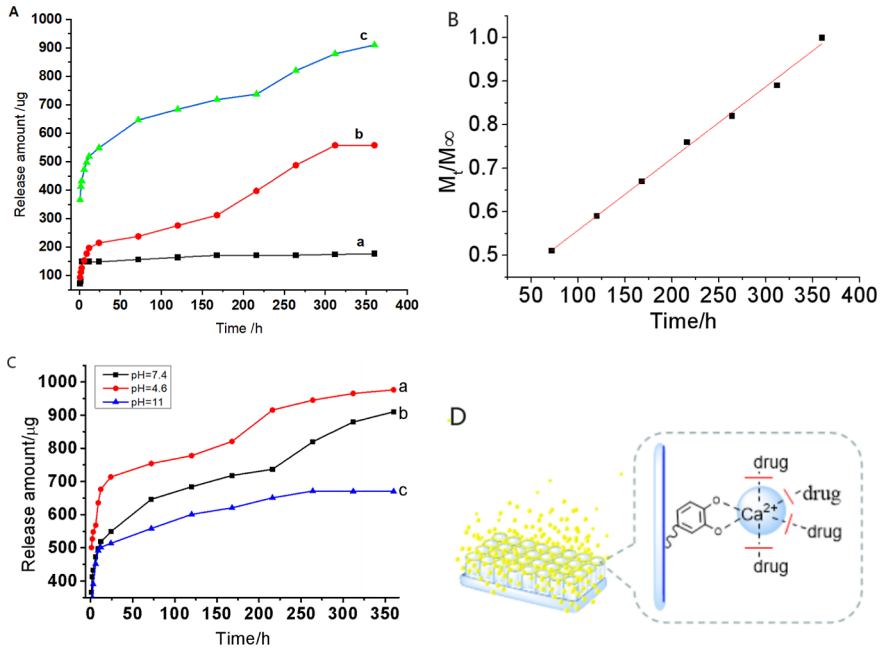

Figure 6. (A) Drug release profiles from different samples at pH = 7.4: (a) TNTs-NaAL, (b) TNTs-PDA-NaAL, and (c) TNTs-PDA-Ca^{2+}-NaAL. (B) Kinetic fitting of the sustained release stage for TNTs-PDA-Ca^{2+}-NaAL at pH = 7.4. (C) Drug release profiles of TNTs-PDA-Ca^{2+}-NaAL at different pH values: (a) 4.6, (b) 7.4, and (c) 11.0. (D) Schematic diagram of the cleavage of the coordination bond between NaAL and Ca^{2+}.

be seen from Figure 6C, a decrease in the pH value of the PBS solution increased the drug release rate. At pH = 4.6, significant drug release was observed from TNTs-PDA-Ca^{2+}-NaAL. This was due to the acidity (pH = 4.6) that cleaved the coordination bonds between Ca^{2+} and NaAL, thereby increasing the free drug molecules released from TNTs-PDA-Ca^{2+}. In contrast, a slower release rate was observed in neutral or alkaline environments (pH 7.4 and pH = 11.0). This suggests that the coordination bonds between Ca^{2+} and NaAL were stable under neutral or alkaline conditions. In summary, the drug was loaded onto TNTs-PDA-Ca^{2+} and achieved a sustained release.

TNTs-PDA-Ca^{2+}-NaAL were immersed in a PBS solution at pH 7.4 and shaken for 15 days to investigate the release behavior of calcium ions. The content was determined by inductively coupled plasma emission spectroscopy. The total amount of loaded calcium ions was 6.86 mg, of which only 2.6% was released after 15 days. Thus, the toxicity of the TNTs-PDA-Ca^{2+}-NaAL was negligible due to the minimal release of calcium ions. This indicated that the rapid release of NaAL at pH 4.6 occurred as a result of coordination bond cleavage between NaAL and Ca^{2+}, as demonstrated in Figure 6D.

3.3. Mineralization. The bioactivity of biomaterial surfaces can be assessed by the formation of hydroxyapatite (HA), a mineral similar to bone that efficiently bonds with bone tissues.[34−37] To assess bioactivity, the samples were mineralized in 1.5 SBF. Surface morphologies of distinct samples were analyzed using FE-SEM after 5 days of mineralization in 1.5 SBF. Scanning electron microscopy (SEM) images (Figure 7) indicated the formation of a mineralized HA layer on both TNTs and TNTs-PDA-Ca^{2+}. The surfaces of the TNTs were partially covered by a thin HA layer (see Figure 7a), whereas numerous mineralized HA nanospheres were highly concentrated on the TNT-PDA-Ca^{2+} surface (see Figure 7b). The results show that TNTs-PDA-Ca^{2+} have a better mineralization

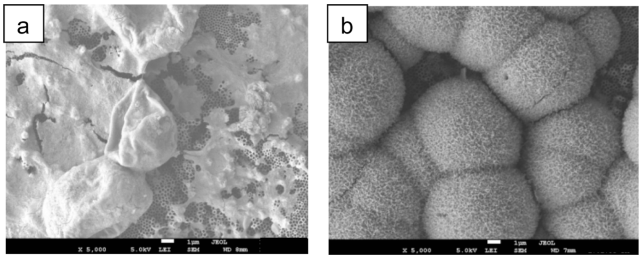

Figure 7. SEM images of (a) TNTs and (b) TNTs-PDA-Ca^{2+} after 5 days of mineralization in 1.5 SBF.

capability compared to pure TNTs primarily because Ca^{2+} can induce the nucleation of HA for its subsequent growth. Moreover, the free catecholamine moieties and negative surface charge of PDA can accelerate the formation of HA.[38,39] Upon soaking in SBF solution, the interaction of PDA functional groups with calcium ions at the nucleation sites leads to the steady deposition of phosphate groups for the growth of the calcium phosphate layer.

3.4. Cytocompatibility Evaluation. The CCK-8 assay was conducted to evaluate the cytotoxicity of the samples. MC3T3-E1 cells were cocultivated with various samples for 1 and 5 days. Figure 8 shows the cell cytocompatibility results. Following 1 day of incubation, TNTs-PDA-Ca^{2+} exhibited slight toxicity, likely resulting from the sudden discharge of free Ca^{2+}. After 5 days of incubation, the cell cytocompatibility significantly increased on all substrates compared to the results after 1 day, which suggests the biocompatibility of the samples without any apparent toxicity to the cells. Figure 8 reveals that, compared with TNTs, the surfaces of TNTs-PDA-Ca^{2+} managed to capture more cells by exploiting the functionalization with PDA and Ca^{2+} that strengthened the samples' bioactivity. The higher biocompatibility shown by samples loaded with NaAL may be related to the presence of the P element in the drug.

https://doi.org/10.1021/acsomega.3c08772
ACS Omega 2024, 9, 4949−4956

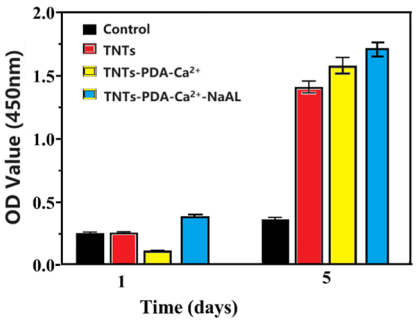

Figure 8. In vitro biocompatibility evaluation of different samples with MC3T3-E1 cell incubation after 1 and 5 days.

4. CONCLUSIONS

To summarize, we successfully created a long-lasting drug delivery system using TNTs by depositing a uniform PDA layer on their surface through a simple ultrasonic method. The TNTs were then modified with calcium ions covalently bonded to NaAL. The drug release results indicated that PDA-modified Ca^{2+}-doped TNTs showed a higher drug loading capacity and release performance when compared to pure TNTs. Furthermore, the results from both the mineralization and cell viability assays demonstrated the improved bioactivity of TNTs-PDA-Ca^{2+}.

AUTHOR INFORMATION

Corresponding Authors

Tao Zhang − *Department of Orthopedics, Fuzhou Second Hospital, Fuzhou, Fujian 350007, China*; Email: tzhang78@126.com

Hong Zheng − *Department of Orthopedics, Fuzhou Second Hospital, Fuzhou, Fujian 350007, China*; Email: hongfsh@163.com

Xiufeng Xiao − *Fujian Provincial Key Laboratory of Advanced Materials Oriented Chemical Engineering, College of Chemistry and Material Science, Fujian Normal University, Fuzhou, Fujian 350007, China*; orcid.org/0000-0001-7256-3935; Email: xfxiao@fjnu.edu.cn

Authors

Lizhong Wu − *Department of Orthopedics, Fuzhou Second Hospital, Fuzhou, Fujian 350007, China*

Xing Wu − *Department of Orthopedics, Fuzhou Second Hospital, Fuzhou, Fujian 350007, China*

Linzhao Wu − *Department of Orthopedics, Fuzhou Second Hospital, Fuzhou, Fujian 350007, China*

Dongdong Chen − *Department of Orthopedics, Fuzhou Second Hospital, Fuzhou, Fujian 350007, China*

Complete contact information is available at: https://pubs.acs.org/10.1021/acsomega.3c08772

Author Contributions

§L.W. and X.W. contributed equally.

Notes

The authors declare no competing financial interest.

ACKNOWLEDGMENTS

This work was financially supported by Fujian Provincial Clinical Medical Research Center for First Aid and Rehabilitation in Orthopaedic Trauma (2020Y2014), Fujian Natural Science Foundation Project (2022J011316 and 2021J01060), 2022 Guiding project of Fujian Provincial Science and Technology Department (2022D018), Medical Innovation Project of Fujian Provincial Health Commission (2020CXB037), Fuzhou health innovation platform construction project (2021-S-wp2), Fujian Provincial Department of Science and Technology Central Leading Local Science and Technology Development Project (2022L3031), Fuzhou Science and Technology Plan technology innovation platform project (2022-P-018, 2021-S-159, and 2021-S-166), and 2020 Fuzhou health innovation platform construction project (2020-S-wp3).

REFERENCES

(1) Liu, X.; Chu, P. K.; Ding, C. Surface modification of titanium, titanium alloys, and related materials for biomedical applications. *Mater. Sci. Eng., R* **2004**, *47* (3−4), 49−121.

(2) Nie, B.; Ao, H.; Long, T.; Zhou, J.; Tang, T.; Yue, B. Immobilizing bacitracin on titanium for prophylaxis of infections and for improving osteoinductivity: an in vivo study. *Colloids Surf., B* **2017**, *150*, 183−191.

(3) Viceconti, M.; Muccini, R.; Bernakiewicz, M.; Baleani, M.; Cristofolini, L. Large-sliding contact elements accurately predict levels of bone-implant micromotion relevant to osseointegration. *J. Biomech.* **2000**, *33* (12), 1611−1618.

(4) Arciola, C. R.; Campoccia, D.; Montanaro, L. Implant infections: adhesion, biofilm formation and immune evasion. *Nat. Rev. Microbiol.* **2018**, *16* (7), 397−409.

(5) Bjursten, L. M.; Rasmusson, L.; Oh, S.; Smith, G. C.; Brammer, K. S.; Jin, S. Titanium dioxide nanotubes enhance bone bonding in vivo. *J. Biomed. Mater. Res., Part A* **2010**, *92A* (3), 1218−1224.

(6) Al-Mobarak, N.; Al-Swayih, A. Development of titanium surgery implants for improving osseointegration through formation of a titanium nanotube layer. *Int. J. Electrochem. Sci.* **2014**, *9*, 32−45.

(7) Peng, L.; Mendelsohn, A. D.; Latempa, T. J.; Yoriya, S.; Grimes, C. A.; Desai, T. A. Long-term small molecule and protein elution from TiO_2 nanotubes. *Nano Lett.* **2009**, *9* (5), 1932−1936.

(8) Wang, Q.; Huang, J.-Y.; Li, H.-Q.; Zhao, A. Z. J.; Wang, Y.; Zhang, K. Q.; Sun, H. T.; Lai, Y. K. Recent advances on smart TiO_2 nanotube platforms for sustainable drug delivery applications. *Int. J. Nanomed.* **2016**, *12*, 151−165.

(9) Moseke, C.; Hage, F.; Vorndran, E.; Gbureck, U. TiO_2 nanotube arrays deposited on Ti substrate by anodic oxidation and their potential as a long-term drug delivery system for antimicrobial agents. *Appl. Surf. Sci.* **2012**, *258* (14), 5399−5404.

(10) Hamlekhan, A.; Sinha-Ray, S.; Takoudis, C.; Mathew, M. T.; Sukotjo, C.; Yarin, A. L.; Shokuhfar, T. Fabrication of drug eluting implants: study of drug release mechanism from titanium dioxide nanotubes. *J. Phys. D: Appl. Phys.* **2015**, *48* (27), 275401.

(11) Gulati, K.; Ramakrishnan, S.; Aw, M. S.; Atkins, G. J.; Findlay, D. M.; Losic, D. Biocompatible polymer coating of titania nanotube arrays for improved drug elution and osteoblast adhesion. *Acta Biomater.* **2012**, *8* (1), 449−456.

(12) Aw, M. S.; Gulati, K.; Losic, D. Controlling drug release from titania nanotube arrays using polymer nanocarriers and biopolymer coating. *J. Biomaterials Nanobiotechnol.* **2011**, *02* (05), 477−484.

(13) Aw, M. S.; Addai-Mensah, J.; Losic, D. Magnetic-responsive delivery of drug-carriers using titania nanotube arrays. *J. Mater. Chem.* **2012**, *22* (14), 6561−6563.

(14) Aw, M. S.; Addai-Mensah, J.; Losic, D. Polymer Micelles for Delayed Release of Therapeutics from Drug-Releasing Surfaces with Nanotubular Structures. *Macromol. Biosci.* **2012**, *12* (8), 1048−1052.

(15) Zhao, J.; Xu, J.; Jian, X.; Xu, J.; Gao, Z.; Song, Y. Y. NIR light-driven photocatalysis on amphiphilic TiO2 nanotubes for controllable drug release. *ACS Appl. Mater. Interfaces* **2020**, *12* (20), 23606−23616.

(16) Yang, Y.; Li, X.; Qiu, H.; Li, P.; Qi, P.; Maitz, M. F.; You, T.; Shen, R.; Yang, Z.; Tian, W.; et al. Polydopamine modified TiO2 nanotube arrays for long-term controlled elution of bivalirudin and

https://doi.org/10.1021/acsomega.3c08772
ACS Omega 2024, 9, 4949−4956

improved hemocompatibility. *ACS Appl. Mater. Interfaces* **2018**, *10* (9), 7649−7660.
(17) Cheng, L.; Sun, X.; Zhao, X.; Wang, L.; Yu, J.; Pan, G.; Li, B.; Yang, H.; Zhang, Y.; Cui, W. Surface biofunctional drug-loaded electrospun fibrous scaffolds for comprehensive repairing hypertrophic scars. *Biomaterials* **2016**, *83*, 169−181.
(18) Lee, H.; Dellatore, S. M.; Miller, W. M.; Messersmith, P. B. Mussel-inspired surface chemistry for multifunctional coatings. *Science* **2007**, *318* (5849), 426−430.
(19) Jiang, L.; Yao, H.; Luo, X.; Zou, D.; Dai, S.; Liu, L.; Yang, P.; Zhao, A.; Huang, N. Polydopamine-modified copper-doped titanium dioxide nanotube arrays for copper-catalyzed controlled endogenous nitric oxide release and improved re-endothelialization. *ACS Appl. Bio Mater.* **2020**, *3* (5), 3123−3136.
(20) Khoshnood, N.; Zamanian, A.; Massoudi, A. Mussel-inspired surface modification of titania nanotubes as a novel drug delivery system. *Mater. Sci. Eng., C* **2017**, *77*, 748−754.
(21) Toita, R.; Toita, R.; Tsuru, K.; Ishikawa, K. Immobilization of calcium and phosphate ions improves the osteoconductivity of titanium implants. *Mater. Sci. Eng., C* **2016**, *68*, 291−298.
(22) Niu, X.; Fan, R.; Tian, F.; Guo, X.; Li, P.; Feng, Q.; Fan, Y. Calcium concentration dependent collagen mineralization. *Mater. Sci. Eng., C* **2017**, *73*, 137−143.
(23) Wang, F.; Cao, B.; Mao, C. Bacteriophage bundles with prealigned Ca^{2+} initiate the oriented nucleation and growth of hydroxylapatite. *Chem. Mater.* **2010**, *22* (12), 3630−3636.
(24) Jiang, H.; Xia, Q.; Liu, D.; Ling, K. Calcium-cation-doped polydopamine-modified 2D black phosphorus nanosheets as a robust platform for sensitive and specific biomolecule sensing. *Anal. Chim. Acta* **2020**, *1121*, 1−10.
(25) Gertz, B.; Holland, S.; Kline, W.; Matuszewski, B. K.; Porras, A. G. Clinical pharmacology of alendronate sodium. *Osteoporosis Int.* **1993**, *3* (S3), 13−16.
(26) Sánchez-Fernández, M. J.; Immers, M. R.; Félix Lanao, R. P.; Yang, F.; Bender, J. C. M. E.; Mecinović, J.; Leeuwenburgh, S. C. G.; van Hest, J. C. M. Alendronate-functionalized poly (2-oxazoline) s with tunable affinity for calcium cations. *Biomacromolecules* **2019**, *20* (8), 2913−2921.
(27) Luo, R.; Tang, L.; Zhong, S.; Yang, Z.; Wang, J.; Weng, Y.; Tu, Q.; Jiang, C.; Huang, N. In vitro investigation of enhanced hemocompatibility and endothelial cell proliferation associated with quinone-rich polydopamine coating. *ACS Appl. Mater. Interfaces* **2013**, *5* (5), 1704−1714.
(28) Oz, U. C.; Küçüktürkmen, B.; Devrim, B.; Saka, O. M.; Bozkir, A. Development and optimization of alendronate sodium loaded PLGA nanoparticles by central composite design. *Macromol. Res.* **2019**, *27* (9), 857−866.
(29) Ochiuz, L.; Grigoras, C.; Popa, M.; Stoleriu, I.; Munteanu, C.; Timofte, D.; Profire, L.; Grigoras, A. Alendronate-loaded modified drug delivery lipid particles intended for improved oral and topical administration. *Molecules* **2016**, *21* (7), 858.
(30) Chen, S.; Luo, Z.; Wu, L.; Xie, C.; Xiao, X. Amino-modified polylactic acid nanofibre microspheres as drug sustained release carriers for alendronate. *Polym.-Plast. Technol. Eng.* **2018**, *57* (18), 1873−1881.
(31) Singhvi, G.; Singh, M. In-vitro drug release characterization models. *Int. J. Pharm. Stud Res.* **2011**, *2* (1), 77−84.
(32) Paarakh, M. P.; Jose, P. A.; Setty, C.; et al. Release kinetics-concepts and applications. *Int. J. Pharm. Res. Technol.* **2018**, *8* (1), 12−20.
(33) Wojcik-Pastuszka, D.; Krzak, J.; Macikowski, B.; Berkowski, R.; Osiński, B.; Musiał, W. Evaluation of the release kinetics of a pharmacologically active substance from model intra-articular implants replacing the cruciate ligaments of the knee. *Materials* **2019**, *12* (8), 1202.
(34) Wu, C.; Chang, J.; Ni, S.; Wang, J. In vitro bioactivity of akermanite ceramics. *J. Biomed. Mater. Res., Part A* **2006**, *76A* (1), 73−80.
(35) Fan, Z.; Wang, J.; Wang, Z.; Li, Z.; Qiu, Y.; Wang, H.; Xu, Y.; Niu, L.; Gong, P.; Yang, S. Casein phosphopeptide-biofunctionalized graphene biocomposite for hydroxyapatite biomimetic mineralization. *J. Phys. Chem. C* **2013**, *117* (20), 10375−10382.
(36) Cui, J.; Ma, C.; Li, Z.; Wu, L.; Wei, W.; Chen, M.; Peng, B.; Deng, Z. Polydopamine-functionalized polymer particles as templates for mineralization of hydroxyapatite: biomimetic and in vitro bioactivity. *RSC Adv.* **2016**, *6* (8), 6747−6755.
(37) Kong, L.; Gao, Y.; Lu, G.; Gong, Y.; Zhao, N.; Zhang, X. A study on the bioactivity of chitosan/nano-hydroxyapatite composite scaffolds for bone tissue engineering. *Eur. Polym. J.* **2006**, *42* (12), 3171−3179.
(38) Ghorbani, F.; Zamanian, A.; Behnamghader, A.; Daliri-Joupari, M. Bone-like hydroxyapatite mineralization on the bio-inspired PDA nanoparticles using microwave irradiation. *Surface. Interfac.* **2019**, *15*, 38−42.
(39) Ding, Y.; Floren, M.; Tan, W. Mussel-inspired polydopamine for bio-surface functionalization. *Biosurface Biotribology* **2016**, *2* (4), 121−136.

https://doi.org/10.1021/acsomega.3c08772
ACS Omega 2024, 9, 4949−4956